JOURNAL OF MATERIALS SCIENCE **40** (2005) 3629–3633

Microstructure and properties of the TiC/Fe-based alloy hardfacing layers

X. H. WANG*, Z. D. ZOU, S. Y. QU, S. L. SONG
School of Materials Science and Engineering, Shandong University, Jinan 250061, People's Republic of China
E-mail: xinhongwang@sdu.edu.cn

TiC/Fe-based alloy hardfacing layers were obtained by shielded metal arc welding (SMAW), in which H08A bare electrode was coated with a powder mixture of ferrotitanium, rutile, graphite, calcium carbonate and calcium fluoride. TiC particles are produced by direct metallurgical reaction between ferrotitanium and graphite during welding. The particles of TiC with cubic shape are distributed evenly in the Fe-rich matrix in the hardfacing layers, the particle size is about 3–5 μm. The microstructure and mechanical properties of the hardfacing layers are markedly affected by the amounted of the ferrotitanium and graphite in the coating of the electrode. The wear properties of the hardfacing layers are superior to the substrate AISI 1045 steel. The coefficient of friction data of the hardfacing layers do not show significant fluctuations.

1. Introdution

Wear related failure of machinery components is one of the most common problems in engineering applications. Wear resistant of materials can be improved through surface modification. There are various surface modification techniques, such as plasma spraying, thermal spraying, hardfacing, laser cladding, chemical and physical vapor deposition processes [1–6]. Hardfacing applications for wear control vary widely, ranging from very severe abrasive, such as rock crushing and pulverizing, to application to minimize metal- to-metal wear, such as control valves, where a few thousands of an inch of wear is intolerable [7].

Metal matrix composite coatings have been known to have high hardness and exceptional wear resistance [8]. Carbide particles have often been incorporated in a Fe matrix to form a composite due to its inherent high hardness. By careful selection of the type of carbides, it is possible to design a composite coating for severe wear conditions. Ceramic particles of TiC have higher hardness and thermal stability than chromium carbides and tungsten carbides [9]. It has been frequently used as reinforcement in Fe-based composite coating [10]. Recent years, TiC reinforced Fe-based composites have been received interest worldwide, but intense research and development are focused on the powder metallurgy routes or liquid-based routes [11–13], there is limited research on the formation of TiC particles via direct metallurgical reaction between FeTi and graphite during arc welding.

The aim of the present investigation is to produce a TiC/Fe-based alloy hardfacing layer by shielded metal arc welding (SMAW). TiC particles were formed by metallurgical reaction of ferrotitanium (FeTi) and graphite during welding, rather than the TiC particles being directly added into the welding pool. The process, microstructure and wear properties of the hardfacing layers were studied to obtain an experimental basis for practical application of TiC/Fe-based alloy surface composite layers.

2. Experimental procedures

The core wire of the electrode was H08A bare electrode with diameter 4 mm, it was coated by a layer of marble-fluorspar-graphite with (wt%) 35–40 ferrotitanium (FeTi), 25–30 rutile (TiO_2), 6-10 calcium carbonate ($CaCO_3$), 10–14 calcium fluoride (CaF_2) and 8–12 graphite (purity 99.5%), 1–2 alkali carbonate and 3–5 other arc-stabilizer. The chemical compositions of H08A, ferrotitanium are shown in Table I. During the welding process, sublimation of graphite and decomposition of $CaCO_3$ in the high temperature produced gas of CO and CO_2, which protected the melting metal and made the arc stability. The alloying elements in the fluxes were transited to the hardfacing layer, thus deposit metals with different alloy contents were obtained.

Hardfacing was done on the substrate AISI 1045 steel plates by using SMAW under direct current with a reverse polarity. The chemical composition of the substrate is shown in Table I. The electrode was baked in the furnace at 250°C for 2 h for drying. To avoid the effect of dilution, hardfacing was welded in a 2 mm thick layer, and then the hardfacings on the second and third layer were done with the same electrode, which were

*Author to whom all correspondence should be addressed.

TABLE I Chemical composition of materials used

Material	Chemical composition (wt%)								
	C	Mn	Si	Cr	Ni	S	P	Ti	Fe
H08A	≤0.10	0.30–0.55	≤0.03	≤0.02	≤0.03	≤0.03	≤0.03	–	Bal.
FeTi	≤0.08	–	–	–	–	≤0.025	≤0.035	≥41.5	Bal.
1045 steel	0.45	0.66	0.25	–	–	≤0.03	≤0.03	–	Bal.

about 3 mm, and with an interpass temperature of about 200–250°C. The welding parameters were as follows: welding current 170–180 A, arc voltage 25–28 V, and electrode traveling speed 0.3–0.4 mm s^{-1}.

Samples were cut from the hardfacing layer using an abrasive cutting machine. Microstructure was observed with an optical microscope (OM), scanning electron microscope (SEM) and transmission electron microscopy (TEM). The chemical composition was analyzed by using electron microprobe analysis (EPMA). The image analyzer (model XQF-2000, China) was used to determine the carbide volume fraction, carbide particle size, distribution and grain size in the hardfacing layer. The structure of the hardfacing layer was analyzed by X-ray diffractometer (XRD). The macrohardness of the hardfacing layer was determined by means of the average of five measurements taken from the surface of the layers.

Tribological properties were performed on testing machine (model: MM-200, China) using block and ring specimens under dry sliding at room temperature. The test specimens were machined into blocks of size of 8 mm ×8 mm ×18 mm. The ring material of the wear couple was a hardmetal containing 92 wt% WC and 8 wt% Co. The wear conditions were 49 N normal load, 0.84 m s^{-1} sliding speed and 750 m sliding distance. The friction coefficient of the layers was recorded in real time by a computerized data acquisition system equipped with an analog/digital converter. The wear resistances were determined by measuring the weight loss after a certain time interval on an analytical balance with a precision of $\pm 10^{-5}$ g. The specimens and ring were removed and cleaned thoroughly in acetone and dried in warm air before measuring the weight loss.

3. Results and discussion

3.1. Thermodynamic analysis and predictions

The thermodynamics of Fe-Ti-C system had been studied by several researchers [14, 15]. It has been concluded that Fe-Ti-C is a complex system due to several factors. For Fe-Ti-C system, it is essential to consider all possible reactions between Ti-C, Fe-Ti and Fe-C. The various reaction equations accompanied by their respective free energy changes for the formation of carbides from respective elemental state is extracted from various sources [16–21], which has been listed in Table II. The free energy values help in predicting the formation of carbides relative to each other.

Fig. 1 shows the Gibbs free energy of formation of the carbide with respect to temperature. It can be seen that the Gibbs free energy of formation of TiC is always

TABLE II Free energy of reaction as function of temperature

Reaction		Free energy (J/mole)	Temperature rage (K)
(1)	$Ti + C = TiC$	$-183172 + 10.09\,T$	298–1155
		$-186731 + 13.20\,T$	1155–2000
(2)	$3Fe + C = Fe_3C$	$25958 - 23.27\,T$	298–463
		$26711 - 24.78\,T$	463–1115
		$10360 - 10.17\,T$	1155–1808
(3)	$2Fe + C = Fe_2C$	$19860 - 10\,T$	298–1155
		$18420 - 10\,T$	1155–1808
(4)	$Ti + 2Fe = Fe_2Ti$	$-53300 + 53.7\,T$	298–2000
(5)	$Ti + Fe = FeTi$	$-39822 + 14.9\,T$	298–2000

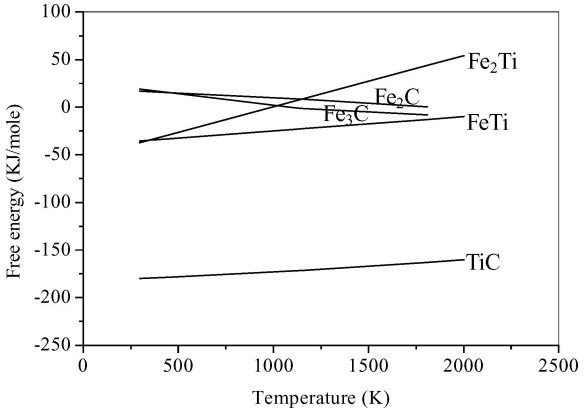

Figure 1 Gibbs free energy of formation of Fe_2Ti, Fe_3C, Fe_2C, FeTi and TiC as a function of temperature.

negative, and its values of TiC is much lower than Fe_3C, Fe_2C and Fe_2Ti. On the other word, Ti has stronger carbide forming tendency than Fe, and TiC has better stability than Fe-C and Fe-Ti. In addition, it also indicates that the free energy of formation of TiC does not change significantly with temperature, it is reasonable to assume that free energy of carbides varies in a similar manner even at the temperature higher than 2000 K during SMAW. Yan *et al.* [19] reported that for Fe-Ti-C system, formation in situ TiC took place only when it has heated to 1373 K. In the welding molten pool, the temperature is much higher than 1373 K, which favors the formation of TiC. Hence, It is evident that formation of TiC by reaction between FeTi and C is possible to occur during SMAW.

It is also indicated from Fig. 1 that some possibility of formation of Fe_3C exists at the temperature over 1100 K. Apart from the temperature, activity of carbon also plays an important role. The coating of the electrode contains lots of graphite and TiC formation occurred with Ti depletion from the Fe-Ti-C system, which could lead to the tendency of Fe reacting with

redundant graphite to form Fe_3C. In addition, it also shows that the formation of Fe_2Ti exists at temperature lower than 1000 K. However, due to formation of TiC and use as deoxidization, Ti is depleted completely during SMAW, there is impossibility of formation of Fe_2Ti.

3.2. Microstructural characteristics

Fig. 2 shows an XRD pattern of the hardfacing layer for the electrode containing 35% FeTi, 25% TiO_2 and 12% graphite. This pattern of the hardfacing layer shows that the products include TiC, Fe_3C, α-Fe and γ-Fe, but no trace of Fe_2Ti and Fe_2C phase remain after the metallurgical reaction. It clearly confirms that TiC particles can be synthesized by direct metallurgical reaction between ferrotitanium and graphite during the welding.

Fig. 3 shows the microstructures of the hardfacing layer. It can be seen that titanium carbide particles are round and distributed evenly in the matrix. Although some areas show more TiC particles than others, the distribution of TiC particles is, in general, uniform. On the surface of the sample, uniform TiC dispersions of 10.4–15.6% by volume fraction are achieved with particle sizes in the range 3–5 μm. Fig. 4 shows the results of EPMA area analysis of elements Ti and C in the hardfacing layer. It indicates that the expected microstructure, well-distributed fine TiC reinforcement in an iron matrix, had been achieved.

Due to the high cooling rate of the SMAW processing, metastable phases, such as martensite and retained austenite etc., are formed. Fig. 5a shows the carbide TEM morphology in the hardfacing layer. It indicates that there is considerable dislocation in the subcrystal structure. Fig. 5b shows the lath martensite and retained austenite in the hardfacing layer, but no twin martensite is found based on the TEM observation. When the lath martensite is formed, the microstructure of the hardfacing layer has high strength and toughness is still largely maintained.

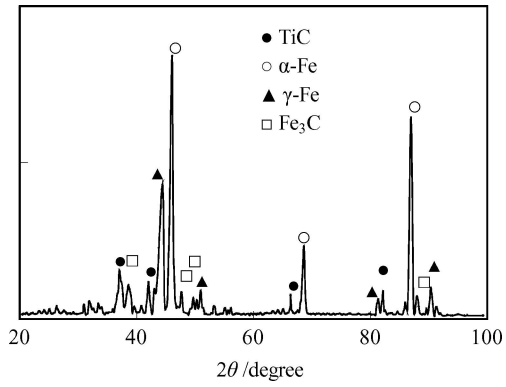

Figure 2 X-ray diffraction spectra of hardfacing layer.

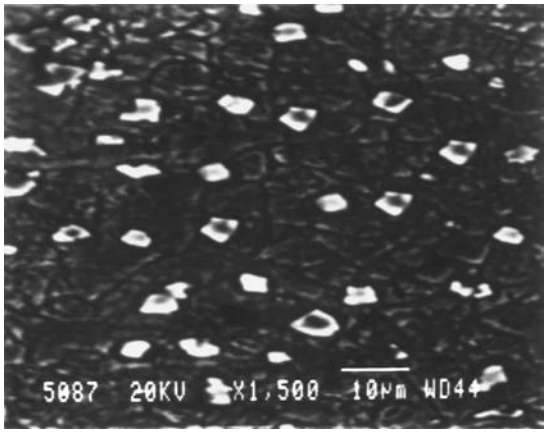

Figure 3 Distribution of TiC particles in the hardfacing layer.

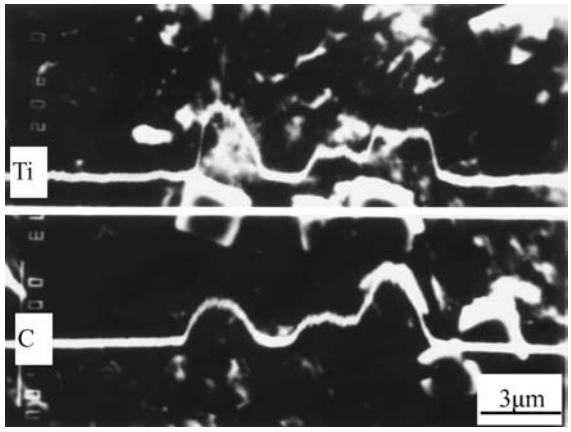

Figure 4 EPMA profiles of Ti and C elements in the hardfacing layer.

The impact fractograph of the hardfacing layer is shown in Fig. 6. It is found that there are a lot of dimples in the impact fractograph. It is possible that such fine dimples be related to the fine particles detected in Fig. 3 and implies that the hardfacing layer possesses good impact toughness. However, when graphite in the coating of the electrode amounted to over 15%, the fracture morphology in the hardfacing layer is a quasi-cleavage fracture, which has a river pattern feature, and shows characteristics of a brittleness fracture (Fig. 6b), and TEM observation found obvious twin martensite and cementite in the hardfacing layer. Therefore, the amount of graphite in the electrode coating should be controlled strictly.

3.3. Hardness of the hardfacing layer

The investigation showed that the key factor affecting the structure, quantity of TiC and properties of the hardfacing layer was the coating composition of the electrode. Fig. 7 shows the relationship between the macrohardness of the hardfacing layers and content of the coating materials. It can be seen that the macrohardness increases rapidly with the increase in the content of graphite in the coating of the electrode. However, based on the observation of SEM, a large quantity of continuous cementite and retained austenite form when graphite amounts to over 12%. With the increase of retained austenite, the hardness of the hardfacing layer decreases. On the other hand, with an increase in the amount of cementite, the crack resistance of the hardfacing layer reduces. Therefore, the amount of graphite should be kept within 10–12%. Ti is a strong carbide-forming element. With an increase in the amount of FeTi, metallurgical reaction formation of TiC increases in the hardfacing layers, as a result the hardness increases. However, the detachability and fluidity of the

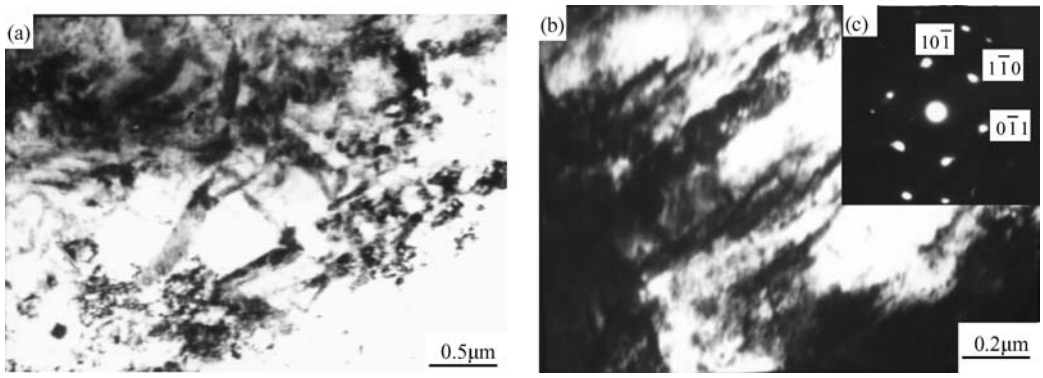

Figure 5 TEM morphology (a) carbides; (b) lath martensite; (c) electron diffraction pattern of martensite.

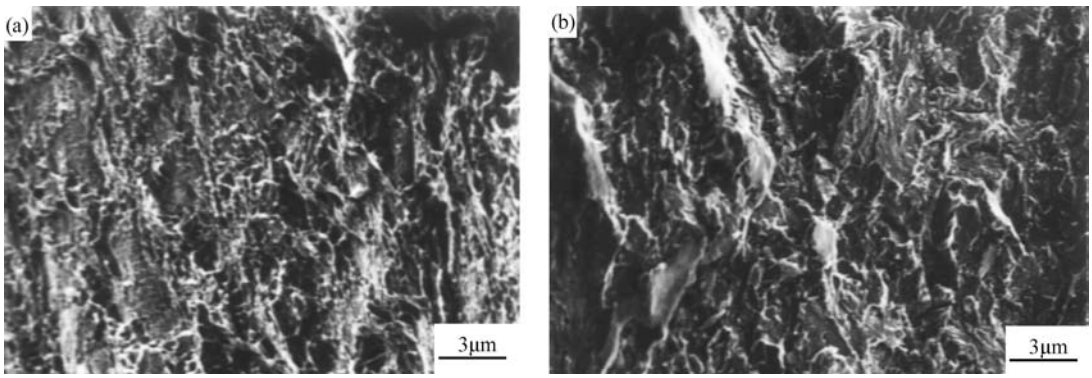

Figure 6 SEM fractograph of hardfacing layers (a) 12% graphite in the coating of the electrode; (b) 15% graphite in the coating of the electrode.

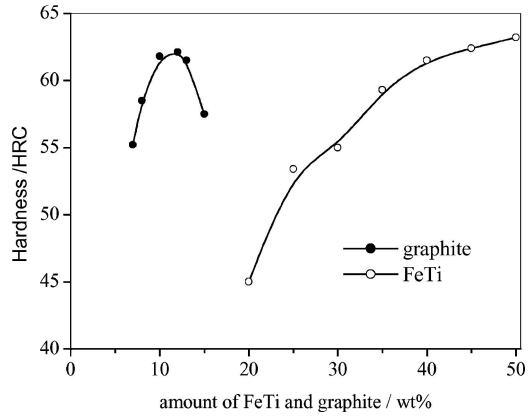

Figure 7 Effect of the amount of FeTi and graphite on the hardness of the hardfacing layer.

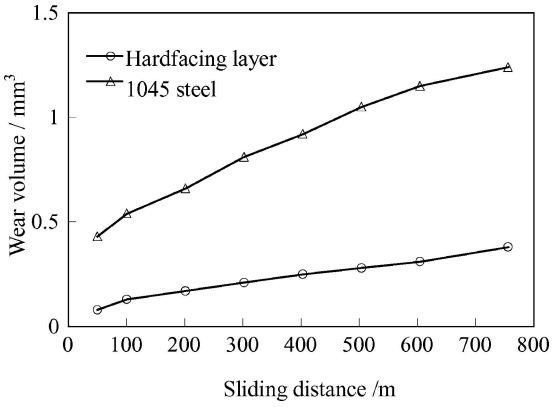

Figure 8 Wear volume vs. the sliding distance.

slag become bad when the amount of FeTi in the coating of the electrode is over 40%. Hence, the amount of the FeTi in the coating of the electrode should be controlled within 40%.

3.4. Wear test

Typical plots of wear volume of the hardfacing layer and AISI 1045 steel substrate as a function of the sliding distance at an applied load of 49 N is shown in Fig. 8. It can be easily observed that the hardfacing layer shows excellent wear resistance compared with to 1045 steel substrate. Additionally, it can also be seen that with an increase of the sliding distance the wear volume increases.

The coefficient of friction versus sliding time for the hardfacing layer and 1045 steel are shown in Fig. 9 at a normal load of 49N and under same test conditions. It shows that the friction coefficient of hardfacing layer is much lower than that of the steel substrate, and the coefficient of friction data of the hardfacing layer does not show significant fluctuations. In addition, the friction coefficient shows fluctuation in value during the wear. This is suggested on the basis of a stick and slip mechanism [22]. As the asperities adhere during the wear, the moving parts stick leading to a high friction value. But, as the junction ruptures under the applied load the friction tends to decrease.

Fig. 10 shows a SEM micrograph of the worn surface of the hardfacing layer. It indicates that there is a mild wear with fine scratches for the hardfacing layer, and there is no indication of brittle failure or loose debris

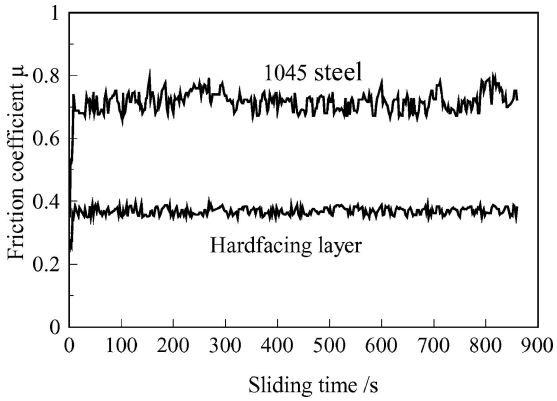

Figure 9 The average coefficient of friction vs. sliding time for the hardfacing layer and 1045 steel.

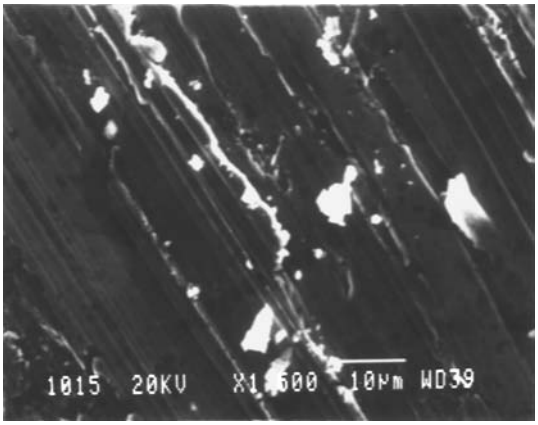

Figure 10 SEM micrograph of the worn surface of hardfacing layer.

formation of TiC ceramic phase. As mentioned earlier, TiC particles in the Fe-based matrix are formed in an metallurgy reaction manner, which improves the bonding strength between the TiC particles and Fe-based matrix interface. As a result the hard TiC particles do not easily pulled out from the matrix during dry sliding. Therefore, TiC/Fe-based hardfacing layer is found to possess a much higher resistance to plastic deformation and scoring, which increases the resistance to plastic erasing and removal of the edges of grooves during subsequent passes.

4. Conclusions

(1) After adding FeTi, TiO_2 and graphite to the coating of an electrode, TiC particles are formed by metallurgical reaction during the arc welding. The microstructure and properties of the hardfacing layer is affected by the amount of FeTi and graphite in the coating of the electrode.

(2) TiC particles are found to distribute evenly in the matrix, the particle size is about 3–5 μm. There are a lot of dimples in the impact fractograph of the hardfacing layer, and shows the characteristic of ductile/tough rupture.

(3) TiC/Fe-based hardfacing layer is found to possess better wear resistance and lower coefficient of friction than that of AISI 1045 steel substrate.

Acknowledgements

The author acknowledges financial support from the Specialized Research Fund for the Doctoral Program of Higher Education (No. 20020422032), the Natural Science Foundation of Shandong Provience (Z2000F02) and Youth Foundation of Shandong University.

References

1. M. YAN, *Surf. Coat. Technol.* **99** (1998) 132.
2. A. KARIMI and CH. VERDON, *ibid.* **62** (1993) 493.
3. A. K. JHA, B. K. PRASAD, R. DASGUPTA and O. P. MODI, *J. Mater. Eng. Perf.* **8** (1999) 190.
4. B. D. ZHU, X. Y. ZENG, Z. Y. TAO, S. G. YANG and K. CUI, *Wear* **170** (1993) 161.
5. S. XIE, W. LI, Z. PAN, B. CHANG and L. SUN, *Mater. Sci. Eng. A* **286** (2000) 11.
6. DOUGLAS E. WOLFE, JOGENDER SINGH and KRISHNAN NARASIMHAN, *Surf. Coat. Technol.* **160** (2002) 206.
7. D. K. DWIVEDI, *Indian Founry Jouranal* **47** (2001) 17.
8. O. Z. OLIN, E. B. JOSEPH and M. CHRIS, *Welding J.* **77** (1998) 43.
9. D. N. NOBLE, *Metal Construction* (1985) 605.
10. S. ECONOMOU, M. DE BONTE, J. P. CELIS, R. W. SMITH and E. LUGSCHEIDER, *Wear*, **220** (1998) 34.
11. R. K. GALGALI, H. S. RAY and A. K. CHAKRABARTI, *Mater. Sci. Technol.* **14** (1998) 810.
12. O. YILMAZ and H. TURBAN, *Comp. Sci. Techn.* **61** (2001) 2349.
13. X. D. HUI and Y. S. YANG, *J. Mater. Sci. Lett.* **19** (2000) 1281.
14. S. JONSSON, *Metall. Mater. Trans. B* **29** (1998) 371.
15. C. RAGHUNATH, M. S. BHAT and P. K. ROHATGI, *Comp. Scr. Metall.* **32** (1995) 577.
16. Y. MURAKAMI, H. KIMURA and Y. NISHIMURA, *Trans. Natl. Res. Inst. Met.* **1** (1959) 7.
17. K. O. KNACKE and K. HESSELMANN, "Thermo-Chemical Properties of Inorganic Substances" 2nd, ed. (Springer-Verlag, New York: 1991).
18. W. J. LU, X. N. ZHANG, D. ZHANG, R. J. WU, Y. J. BIAN and P. W. FANG, *Acta Metall. Sinica* **35** (1999) 536.
19. Y. W. YAN, B. K. WEI, Z. Y. FU, H. T. LIN and R. Z. YUAN, *ibid.* **35** (1999) 1117.
20. A. AGARWAL and N. B. DAHOTRE, *J. Mater. Eng. Perf.* **8** (1999) 479.
21. Y. J. LIANG and Y. C. CHE, "Handbook of Data on Abiothermodynamics," (Northeast University Press Shenyang, 1991) (in Chinese).
22. F. P. BOWEN and L. LEBEN, *Proc. R. Soc. A* **169** (1939) 371.

Received 8 November 2004
and accepted 22 February 2005